Small-Amplitude and Mixed-Mode pH Oscillations in the Bromate−Sulfite−Ferrocyanide−Aluminum(III) System

Klara Kovacs, Marcin Leda, Vladimir K. Vanag, and Irving R. Epstein*

Department of Chemistry, Brandeis University, MS 015, Waltham, Massachusetts 02454

Received: September 3, 2008; Revised Manuscript Received: November 3, 2008

The $BrO_3^--SO_3^{2-}-Fe(CN)_6^{4-}$ (BSF) pH-oscillatory system is coupled to the $Al(OH)_3$ precipitation equilibrium (BSFA system) and studied in a stirred flow reactor. The dynamic behavior of the BSFA system differs significantly from that of the BSF system. In addition to the large-amplitude pH oscillations found in the BSF system, new small-amplitude and mixed-mode oscillations occur. A detailed mechanism of the BSFA system is developed and investigated.

Introduction

The family of pH oscillators[1] in which H^+ serves as the autocatalytic activator species is of considerable interest because of potential applications such as artificial muscles,[2−4] controlled drug-delivery systems,[5] and DNA-based nanodevices.[6,7] One pH oscillator, the $Fe(CN)_6^{4-}-IO_3^--SO_3^{2-}$ system, exhibits dissipative patterns (breathing spots,[8] shrinking rings and spirals,[9] self-replicating spots,[10−12] and stationary lamellar patterns[13]) in a continuously fed unstirred reactor (CFUR). These experimental observations suggest the possibility of finding analogous, or even new, patterns in other pH-oscillatory systems.

A method was recently developed[14] to couple a pH oscillator with complexation and precipitation equilibrium reactions to induce oscillations in the concentration of a previously nonoscillatory metal or halogen ion. In this way, periodic changes in, for example, the Al^{3+} or Ca^{2+} concentration can be generated. Because Ca^{2+} is widespread in biological systems, the coupling of a pH oscillator with Ca^{2+} might have important applications.[15] Connecting pH oscillations with precipitation equilibria offers the possibility of pattern formation in reaction−diffusion systems arising from a new mechanism, the state dependence of diffusion coefficients. Indeed, the production and dissolution of a precipitate at different pHs can significantly change the diffusion of species in a system incorporated into a gel matrix.

Herein, we report our results on the bromate−sulfite−ferrocyanide (BSF) system, which we couple to the $Al(OH)_3$ precipitation equilibrium. The BSF system was created by a systematic design algorithm for pH oscillators and shows large-amplitude periodic changes in pH in a continuously stirred tank reactor (CSTR) over a wide range of experimental conditions.[16] Adding Al^{3+} to the BSF system can generate periodic oscillations in the concentration of Al^{3+} ions as a result of the pH-dependent precipitation reaction[17,18]

$$Al^{3+} + 3OH^- \leftrightarrow Al(OH)_3 \qquad (1)$$

Reaction 1 can significantly change the dynamic behavior of the original pH-oscillatory system, depending on the concentration of Al^{3+} added. In some cases, Al^{3+} can induce or suppress pH oscillations. The dynamical behavior of the BSF−Al^{3+} (BSFA) system and the mechanism of its oscillations are the subject of this paper.

* To whom correspondence should be addressed. E-mail: epstein@brandeis.edu.

Experimental Section

The CSTR consisted of a cylindrical water-jacketed Teflon reactor with two glass windows on opposite walls of the reactor. The volume (V_0) of the reactor was 22 mL. A Haake thermostat was used to maintain a constant temperature during experiments. The stock solutions were prepared from reagent-grade $NaBrO_3$, $K_4[Fe(CN)_6]$, Na_2SO_3, H_2SO_4 and $Al(NO_3)_3$ (Fisher) without further purification. The $Fe(CN)_6^{4-}$ solution was prepared one day in advance, refrigerated overnight, and kept in the dark during experiments because of its light sensitivity. Sulfite solutions were used within 3 h of preparation to avoid oxidation to sulfate. The stock solutions were flowed into the reactor by two Gilson peristaltic pumps. The excess solution from the reactor was removed with an aspirator pump. The pH was measured with a combined glass electrode and a pH meter connected to a personal computer. The intensity of transmitted light through the reactor at wavelengths $\lambda \geq 570$ nm was measured with a TIA-525 optical receiver, which is an optical-to-electrical converter. This wavelength range allowed us to monitor optical changes related to the $Al(OH)_3$ precipitate, because $Fe(CN)_6^{4-}$ has negligible absorption above 570 nm. Dynamic light scattering experiments were performed with a DynaPro instrument (Protein Solutions, High Wycombe, U.K.).

Numerical integration of the ordinary differential equations (ODEs) was performed using the package XPPAUT.[19] The method of integration was STIFF, and the tolerance was typically set at 10^{-5}.

Results

Experiments. We first carried out experiments on the BSF system without $Al(NO_3)_3$ to generate "reference" oscillations and parametric (bifurcation) diagrams for comparison with the BSFA system. A bifurcation diagram in the $k_0-[Fe(CN)_4^{6-}]_0$ plane, where $k_0^{-1} = V_0/v$ is the residence time of the reactor and v is the flow rate, is shown in Figure 1a. The plot exhibits the classical cross-shaped form, as expected from previous results on this system.[16] Our experiments were carried out at 28 and 26.5 °C. At 28 °C, the oscillatory region is wider, but the lower temperature, 26.5 °C, provides better conditions for studying the new small-amplitude oscillations that occur in the BSFA system. The large-amplitude oscillations, characteristic of the BSF system, are much less sensitive to small changes in temperature. As shown in Figure 1a, oscillations in the BSF

10.1021/jp807840g CCC: $40.75
Published on Web 12/16/2008

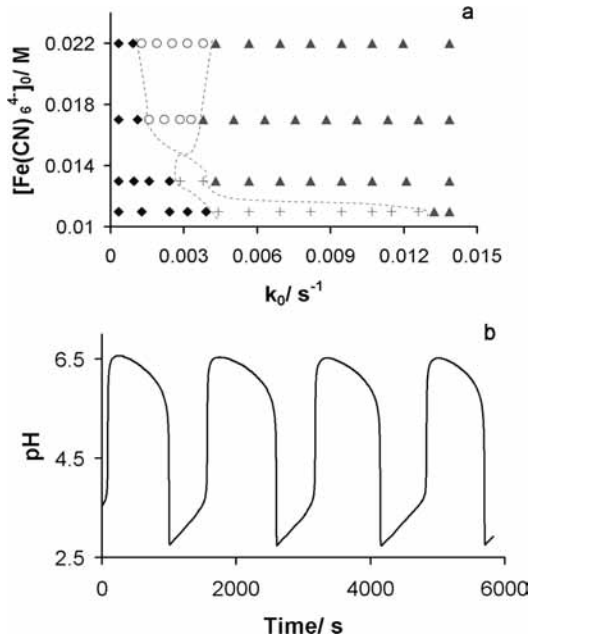

Figure 1. (a) Cross-shaped phase diagram in the $k_0-[Fe(CN)_6^{4-}]_0$ parametric plane for the $BrO_3^- - SO_3^{2-} - Fe(CN)_6^{4-}$ system at $[BrO_3^-]_0 = 0.059$ M, $[SO_3^{2-}]_0 = 0.082$ M, $[H^+]_0 = 0.022$ M, and $T = 28$ °C. Symbols: (◆) SS1, steady-state pH ≈ 3; (▲) SS2, steady-state pH ≈ 6.4; (○) OSC, large-amplitude oscillations (between pH 3 and pH 6.5); (+) BS, bistability between two steady states. (b) pH oscillations at the same conditions as in a with $[Fe(CN)_6^{4-}]_0 = 0.015$ M and $k_0 = 3.15 \times 10^{-3}$ s^{-1}.

system occur for $[Fe(CN)_6^{4-}]_0 \geq f_{cr}$ (= 0.017 M for our chosen concentrations of BrO_3^- and SO_3^{2-}), whereas the bistability region lies at $[Fe(CN)_6^{4-}]_0 < f_{cr}$. In the oscillatory region, regular, large-amplitude pH oscillations occur between pH 3 and pH 6.7 (Figure 1b) with the same shape as reported previously.[16]

The dynamic behavior of the BSF system changes if even a small amount of Al^{3+} [in the form of $Al(NO_3)_3$] is added. Typical examples of three different types of oscillations found in the BSFA system are presented in Figure 2. These are regular, large-amplitude oscillations (Figure 2a) like those in the reference system, mixed-mode oscillations (MMOs) (Figure 2b), and small-amplitude oscillations (Figure 2c). One period of MMO consists of one large-amplitude oscillation (1L) and n (= 1, 2, 3,...) small-amplitude oscillations (nS). In Figure 2b, we see an initial irregular transient behavior followed by (1L + 1S) oscillations.

Figure 3 demonstrates the dynamical behavior of the system in several parametric planes. All of these bifurcation diagrams have a cross-shaped form. The diagram in the $k_0-[Fe(CN)_4^{6-}]_0$ plane (Figure 3a) can be compared to the diagram in Figure 1a. The oscillatory and bistability regions for the BSFA system are slightly shifted to higher values of k_0 relative to those for the BSF system. In the oscillatory region, new small-amplitude and mixed-mode oscillations emerge between the regions of low-pH steady state (SS) and large-amplitude oscillations.

The initial concentration of Al^{3+} ($[Al^{3+}]_0$) has a significant effect on the system, as seen in the $k_0-[Al^{3+}]_0$ plane (Figure 3b). An increase in $[Al^{3+}]_0$ leads to the disappearance of the small-amplitude oscillations and a shift of the large-amplitude pH oscillations to higher flow rates. The range of k_0 in which oscillations occur narrows, and the bistability region lies at higher $[Al^{3+}]_0$ and k_0.

Figure 3c shows the $[Al^{3+}]_0-[Fe(CN)_6^{4-}]_0$ parameter plane. At lower $[Al^{3+}]_0$ and higher initial ferrocyanide concentration

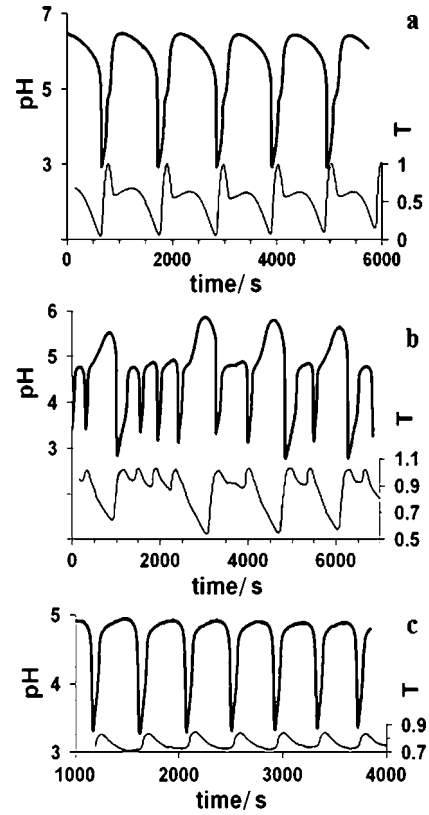

Figure 2. Oscillations in pH and transmittance (T) (arbitrary units) in CSTR experiments. $[BrO_3^-]_0 = 0.059$ M; $[SO_3^{2-}]_0 = 0.082$ M; $[H^+]_0 = 0.022$ M; $[Fe(CN)_6^{4-}]_0 = 0.0017$ M; $T = 26.5$ °C; and k_0/s^{-1} = (a) 0.0047, (b) 0.00286, (c) 0.0025.

($[Fe(CN)_6^{4-}]_0$), only the high-pH SS can be observed. The oscillatory region, including large-amplitude, mixed mode, and small-amplitude pH oscillations, emerges at higher $[Al^{3+}]_0$, and the low-pH SS region lies at still greater $[Al^{3+}]_0$ or at lower $[Fe(CN)_6^{4-}]_0$. At the boundary between the oscillatory and low-pH SS regions, a new bistability regime (marked by the asterisks in Figure 3c) between small-amplitude oscillations and the low-pH SS can be seen. This bistability indicates a subcritical Hopf bifurcation. At small $[Fe(CN)_6^{4-}]_0$ (<0.01 M) and small $[Al^{3+}]_0$ (<0.0018 M), bistability between the low- and high-pH steady states occurs.

To demonstrate the quantitative changes in pH that correspond to the qualitative changes in the dynamical behavior of the BSFA system, we present two bifurcation diagrams in Figure 4. In Figure 4a, which represents a cross section of the oscillatory regions in the $k_0-[Fe(CN)_4^{6-}]_0$ (Figure 3a) or $k_0-[Al^{3+}]_0$ (Figure 3b) plane, with increasing k_0, we see an increase in the pH of the low-pH SS1, followed by the onset of first small-amplitude and then large-amplitude oscillations, and finally the high-pH SS2. This figure demonstrates the sharp jump in the amplitude of pH oscillations between the small- and large-amplitude oscillations.

In Figure 4b, which corresponds to a cross section of the diagram shown in Figure 3b at the "cross point", $[Al^{3+}]_0 = 0.0069$ M, we see that an increase in k_0 leads to a rise in the pH of the low-pH SS (up to pH ≈ 4.5) at relatively small k_0 (as in Figure 4a). Then, however, further increases in k_0 do not affect the steady-state pH over a remarkably wide range of k_0 (from 4×10^{-3} to 1.4×10^{-2} s^{-1}), until the system jumps to the high-pH SS at $k_0 \approx 1.4 \times 10^{-2}$ s^{-1}.

The small-amplitude oscillations are quite sensitive to temperature. Above 29.8 °C, oscillation ceases, and the system

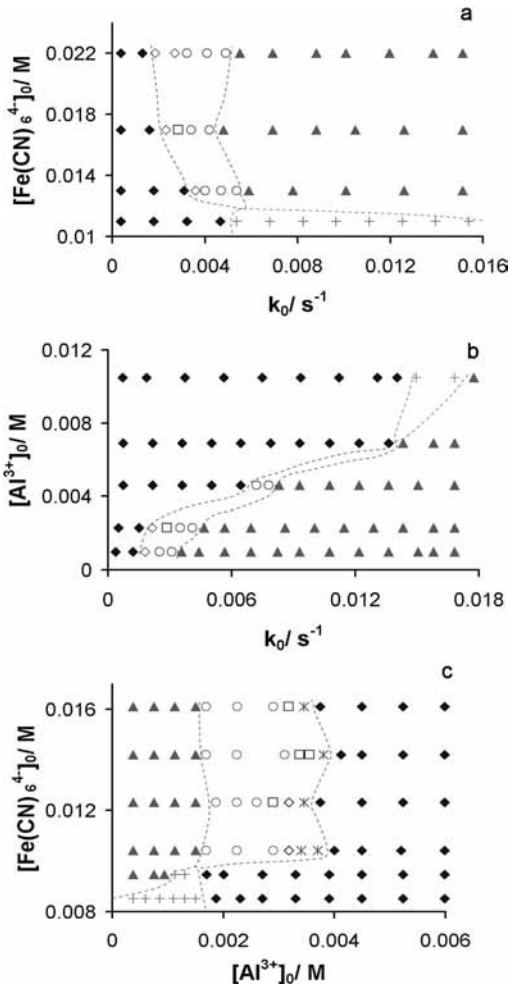

Figure 3. Parametric diagrams for the BSFA system at $T = 26.5$ °C. (a) $k_0-[Fe(CN)_6^{4-}]_0$ plane at $[BrO_3^-]_0 = 0.059$ M, $[SO_3^{2-}]_0 = 0.082$ M, $[H^+]_0 = 0.022$ M, $[Al^{3+}]_0 = 0.0023$ M. (b) $k_0-[Al^{3+}]_0$ plane at $[BrO_3^-]_0 = 0.059$ M, $[SO_3^{2-}]_0 = 0.082$ M, $[H^+]_0 = 0.022$ M, $[Fe(CN)_6^{4-}]_0 = 0.0017$ M. (c) $[Al^{3+}]_0-[Fe(CN)_6^{4-}]_0$ plane at $[BrO_3^-]_0 = 0.0615$ M, $[SO_3^{2-}]_0 = 0.072$ M, $[H^+]_0 = 0.019$ M, $k_0 = 0.0026$ s^{-1}. Symbols: (◆) SS1, steady-state pH ≈ 3; (▲) SS2, steady-state pH ≈ 6.4; (+) BS1, bistability between SS1 and SS2; (◇) OSC1, small-amplitude pH oscillations (pH 3.5−4.5); (□) MMO, mixed-mode oscillations; (○) OSC2, large-amplitude oscillations (pH 3−6.5); (*) BS2 bistability between small-amplitude oscillation (OSC1) and low-pH steady state.

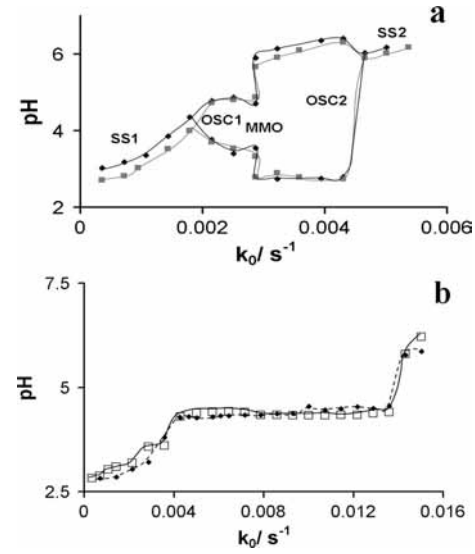

Figure 4. Bifurcation diagrams for the BSFA system. (a) $[BrO_3^-]_0 = 0.059$ M, $[SO_3^{2-}]_0 = 0.082$ M, $[H^+]_0 = 0.022$ M, $[Fe(CN)_6^{4-}]_0 = 0.022$ M, $[Al^{3+}]_0 = 0.0023$ M, $T = 28$ °C. OSC2, small-amplitude oscillations; MMO, mixed-mode oscillations. Maximum and minimum of pH oscillations are shown in the bifurcation diagram at each flow rate. Symbols: (□) increasing k_0, (■) decreasing k_0. (b) Bifurcation diagram showing the monostable system. Parameters correspond to the cross section of the $k_0-[Al^{3+}]_0$ diagram in Figure 3b at $[Al^{3+}]_0 = 0.0069$ M.

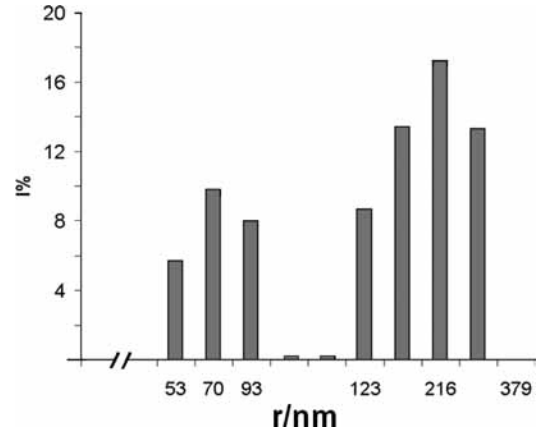

Figure 5. $Al(OH)_3$ particle size distribution. $[SO_3^{2-}] = 0.3$ M, $[Al(NO)_3] = 6 \times 10^{-4}$ M, pH = 4.0.

resides in the low-pH steady state (pH ≈ 4.6). If the temperature is decreased, mixed-mode and large-amplitude oscillations can be induced.

Although we do not study here the complexation and precipitation of $Al(OH)_3$ per se, we monitor the correlation between the pH oscillations and $Al(OH)_3$ precipitation via light transmittance measurements. It is known that $Al(OH)_3$ is dissolved below pH 3.7 and precipitates at higher pH.[20] Because our pH oscillations have their maximum and minimum above and below this pH value, respectively, periodic changes in $[Al(OH)_3]$ (or more accurately, in transmittance) can be observed, as shown in Figure 2. Where the pH has a maximum, the transmittance has a minimum. In the case of large-amplitude oscillations, the transmittance−time curves show that $Al(OH)_3$ production can be more complex, because a secondary maximum also appears. The hydrolysis of aluminum in aqueous systems has been investigated by many researchers in an attempt to understand the complicated processes of polymerization and precipitation of aluminum oxides and hydroxides. For example, Bottero et al.[21] and Packter et al.[17,22] studied Al^{3+} hydrolysis and found that it is possible to produce several crystalline forms of $Al(OH)_3$. With increasing particle size, amorphous, microcrystalline boehmite, and gibbsite forms of the precipitate can be detected. These different types of $Al(OH)_3$ might be responsible for the secondary maximum in the transmittance observed in our experiments. It is possible to obtain different polymer structures as the pH changes, which might also contribute to the appearance of the second maximum.

To assess the size of the precipitate $Al(OH)_3$ particles, we performed dynamic light scattering (DLS) experiments. A typical distribution of particle sizes is shown in Figure 5 for a sulfite solution at pH 4. We see two peaks at approximately $R_1 \approx 70$ nm and $R_2 \approx 200$ nm. We also measured particle size distributions in bromate and ferrocyanide solutions at pH 4 and pH 5. These, too, were bimodal, but with slightly different maxima R_1 and R_2. At higher pH, the particle size distributions shift to higher values, as expected. The average particle size increases with time. Larger particles (in the range of microme-

TABLE 1: Model of the $BrO_3^- - SO_3^{2-} - Fe(CN)_6^{4-} - Al^{3+}$ System[a]

$$3HSO_3^- + BrO_3^- \rightarrow 3H^+ + 3SO_4^{2-} + Br^- \qquad r_2 = k_2[HSO_3^-][BrO_3^-] \quad (2)$$

$$3H_2SO_3 + BrO_3^- \rightarrow 6H^+ + 3SO_4^{2-} + Br^- \qquad r_3 = k_3[H_2SO_3][BrO_3^-] \quad (3)$$

$$6HFe(CN)_6^{3-} + BrO_3^- \rightarrow 6Fe(CN)_6^{3-} + Br^- + 3H_2O \qquad r_4 = k_4[HFe(CN)_6^{3-}][BrO_3^-] \quad (4)$$

$$Al(OH)_2^+ + OH^- \rightarrow Al(OH)_3(s) \qquad r_5 \quad (5)$$

$$Al(OH)_3(s) \rightarrow Al(OH)_2^+ + OH^- \qquad r_6 = k_6 \times \Theta([Al(OH)_3(s)]) \quad (6)$$

$$Al^{3+} + 2OH^- \rightleftarrows Al(OH)_2^+ \qquad K_A \quad (7)$$

$$SO_3^{2-} + H^+ \rightleftarrows HSO_3^- \qquad K_{S1} \quad (8)$$

$$HSO_3^- + H^+ \rightleftarrows H_2SO_3 \qquad K_{S2} \quad (9)$$

$$SO_4^{2-} + H^+ \rightleftarrows HSO_4^- \qquad K_{SA} \quad (10)$$

$$Fe(CN)_6^{4-} + H^+ \rightleftarrows HFe(CN)_6^{3-} \qquad K_F \quad (11)$$

$$OH^- + H^+ \rightleftarrows H_2O \qquad K_w \quad (12)$$

$$6H_2SO_3 + BrO_3^- \rightarrow 6H^+ + 3S_2O_6^{2-} + Br^- + 3H_2O \qquad k_{13} = [H_2SO_3][BrO_3^-] \quad (13)$$

[a] Note: $k_2 = 3.3 \times 10^{-2}$ M^{-1} s^{-1} (this work), $k_3 = 22$ M^{-1} s^{-1},[54] $k_4 = 8.5 \times 10^{-2}$ M^{-1} s^{-1} (this work), $r_5 = k_5[Al(OH)^{2+}][OH^-] \times \Theta([Al(OH)^{2+}][OH^-] - K_p)$, $k_5 = 5 \times 10^8$ M^{-1} s^{-1} (this work), $K_p = 4.68 \times 10^{-16}$ M^2 for $a_{in} < 0.007$ M and 4.68×10^{-15} M^2 for $a_{in} > 0.007$ M,[18,29,31] $k_6 = K_p k_5$, $k_{13} = 0.70$ M^{-1} s^{-1},[24,25] $\Theta(x) = 0$ if $x \leq 0$ and 1 if $x > 0$, $K_A = 7.41 \times 10^{17}$ M^{-2},[18,29] $K_{SA} = 87.1$ M^{-1} ($\log K_{SA} = 1.94$),[54] $K_{S1} = 10^7$ M^{-1} ($\log K_{S1} = 7$), $K_{S2} = 60$ M^{-1} ($\log K_{S2} = 1.78$),[24,25] $K_F = 1667$ M^{-1} ($\log K_F = 3.22$),[31] and $K_w = 10^{14}$ M^{-2}.

ters) are also present and can be seen through a microscope but cannot be detected with our DLS apparatus.

Simulations. In Table 1, we summarize the reaction steps and parameters that we used to simulate the BSFA system. Before presenting the results, we discuss various aspects of our model in more detail.

The reactions in our model can be grouped into four sets, namely, positive feedback (reactions 2 and 3), negative feedback (reaction 4), relatively slow reactions of precipitation and dissolution of $Al(OH)_3$ (reactions 5 and 6), and fast protonation−deprotonation equilibria (reactions 7−12). The slow reaction (reaction 13), an alternative to reaction 3, is also taken into account.

Two mechanisms for positive feedback in the BSF reaction have been proposed in the literature.[16,23] The first takes into account only reaction 2 in Table 1, as well as a series of reactions involving bromine species such as HOBr, Br_2, Br^-, and $HBrO_2$.[16] The second is based on autocatalytic reaction 3 in Table 1, which can be rewritten to emphasize the autocatalysis in H^+ as

$$3H^+ + 3HSO_3^- + BrO_3^- \rightarrow 6H^+ + 3SO_4^{2-} + Br^- \quad (3m)$$

We believe that the second mechanism is more relevant.

Because the value of rate constant k_2 was known only at 35 °C (0.0653 M^{-1} s^{-1}),[24,25] we performed our own experiments on the reaction between sulfite and bromate to determine k_2 at 25 °C. The result is given in the footnote to Table 1. In reaction 4 (which plays the role of a negative feedback),[26,27] the protonated form $HFe(CN)_6^{3-}$ reacts with BrO_3^- relatively quickly, whereas the deprotonated form $Fe(CN)_6^{4-}$ is almost unreactive. Reaction 4 is a complex reaction that consists of several fast and slow steps,[16,27] resulting in the rate law that appears in Table 1.

To describe precipitation reaction 1, we split it into three steps. The first is a rapid hydroxylation equilibrium (reaction 7). The second is the formation of the precipitate $Al(OH)_3(s)$ (reaction 5), and the third is its dissolution (reaction 6). This precipitate can occur in two forms, amorphous and crystalline (gibbsite). The rate of precipitation contains two terms corresponding to nucleation and aggregation steps.[28] Nucleation can be described by a simple Heaviside function $\Theta(x)$, where x is the difference between the concentration in solution, $[Al(OH)_3(aq)]$, and the nucleation concentration of $Al(OH)_3$. The aggregation process can be autocatalytic, because the rate increases as the surface area of the precipitate grows. The dissolution rate must also depend on the size (and surface area) of the crystals, which we cannot characterize in detail. We therefore choose to describe the complex processes of precipitation and dissolution with the simple rate expressions r_5 for precipitation and r_6 for dissolution (see Table 1). The constant K_p in r_5 is obtained from the solubility product K_s of amorphous $Al(OH)_3(s)$ and the equilibrium constant K_A as $K_p = K_s/K_A$, where $K_s = 10^{-33.2}$ M^4.[18,29] The values of k_5 and k_6 are tuned to give oscillations similar to those found in our experiments. Note that we take the rate r_6 for dissolution to be constant as long as some precipitate is present. In reality, however, this rate should depend on the total surface area of precipitate particles.

The full model shown in Table 1 contains 13 variables: $s_0 = [SO_3^{2-}]$, $s_1 = [HSO_3^-]$, $s_2 = [H_2SO_3]$, $b = [BrO_3^-]$, $f_0 = [Fe(CN)_6^{4-}]$, $f_1 = [HFe(CN)_6^{3-}]$, $o = [OH^-]$, $h = [H^+]$, $a_0 = [Al^{3+}]$, $a_2 = [Al(OH)_2^+]$, $p = [Al(OH)_3(s)]$, $m_0 = [SO_4^{2-}]$, and $m_1 = [HSO_4^-]$. To simplify the analysis and provide more insight into the system, we show in Appendix A and Appendix B how to reduce the full model to smaller models that capture the key dynamic features.

We first derive a two-variable model for the BSF system without Al^{3+} (Appendix A). This BSF model (eqs A44 and A45) with variables h and s ($\equiv s_0 + s_1 + s_2$) reproduces quite well the experimental results presented in Figure 1. To approximate the steady states of the BSF model (eqs A44 and A45), we can

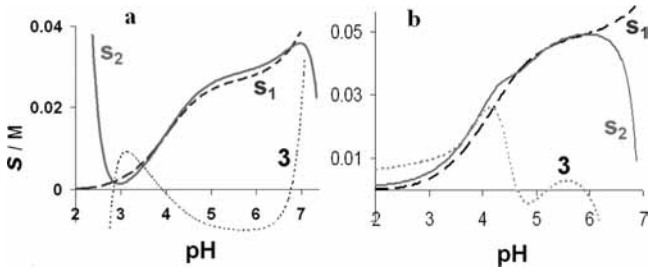

Figure 6. Nullclines for the BSF model (eqs A44 and A45) and the BSFA model (eqs B57−B60) under bistable conditions. (a) Curves $\mathbf{s}_1$ and $\mathbf{s}_2$ were obtained from eqs A44 and A45, respectively, and curve **3** is the difference $k(\mathbf{s}_1 - \mathbf{s}_2)$, where k is an arbitrary scale factor. Parameters: $k_0 = 0.004$ s^{-1}, $k_2 = 6.6 \times 10^{-2}$ M^{-1} s^{-1}, $K_{SA} = 87.1$ M^{-1}, $K_F = 1700$ M^{-1}, $f_{in} = 0.01$ M, $s_{in} = 0.082$ M, $b_{in} = 0.059$ M, $m_{in} = 0.011$ M, and $h_{in} = 0.022$ M. (b) Curves $\mathbf{s}_2$ and $\mathbf{s}_1$ are nullclines obtained from rate equations for h and s, respectively, and curve **3** is the difference between the two nullclines. Parameters: $s_{in} = 0.082$ M, $b_{in} = 0.059$ M, $f_{in} = 0.022$ M, $h_{in} = 0.022$ M, $a_{in} = 0.008$ M, $k_0 = 0.008$ s^{-1}, and $K_p = 4.68 \times 10^{-15}$ M^2.

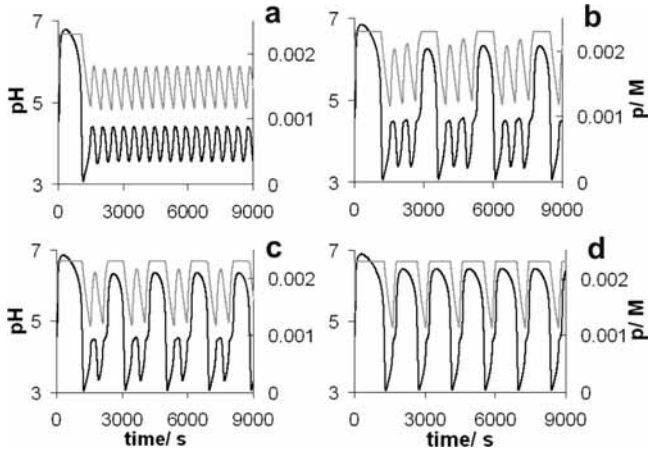

Figure 7. Profiles of pH (black) and precipitate concentration (p) (gray) obtained from eqs B57−B60 for $a_{in} = 0.0023$ M; $K_p = 4.68 \times 10^{-16}$ M^2; and $k_0 =$ (a) 0.0012, (b) 0.00132, (c) 0.00135, and (d) 0.0015 s^{-1}. Other parameters as in Figure 6b.

express the variable s in both eq A44 and eq A45 as a function of h and construct the nullclines, shown in Figure 6a, whose intersections define the bistability region. The steady states (the intersections of the nullclines) found graphically from Figure 6a coincide well with the experimental values in the bistability region. Exact SS values, h_{SS} and s_{SS}, can be found numerically.

We then developed a four-variable model for the BSFA system (see Appendix B). It is possible to derive a three-variable model with variables h, s, and p, if we ignore the slow reaction (eq 13), but this model is unable to reproduce the MMO region shown in Figure 2b with reasonable parameters. We therefore explore our four-variable BSFA model (eqs B57−B60) with variables s, h, p, and m ($\equiv m_0 + m_1$), which takes into account reaction 13.

To find the steady states of the BSFA model, we consider two cases. If $(a_{in} - p)D_5 < K_p$, the rate of precipitation is zero (eq B64), and the left side of eq B59 is negative (zero), if $p > 0$ ($p = 0$). Hence, for $(a_{in} - p)D_5 < K_p$, the precipitate concentration p goes asymptotically to its stationary-state value, $p_{SS} = 0$. The steady-state concentrations of the other variables can be found using eqs B57, B58, and B60, which involve only the components of the BSF system.

If $(a_{in} - p)D_5 > K_p$, the precipitation rate is positive, and the stationary concentration of precipitate can be obtained from eq B59 as

$$p_{SS} = (a_{in}D_5 - K_p)/(k_0/k_5 + D_5) \quad (14)$$

Usually, k_0 is smaller than the precipitation rate constant k_5, so p_{SS} is very close to the influx concentration of aluminum, a_{in}. In either case, the values of h_{SS}, s_{SS}, and m_{SS} must be found numerically.

Similarly to the BSF model, the BSFA model can be analyzed in the (h, s) phase plane, which is a projection of the four-variable phase space (h, s, m, p) to the plane defined by $m = m_{SS}$, $p = p_{SS}$. Figure 6b shows the nullclines of the BSFA model, which intersect at the stable steady states SS1 (pH 4.7) and SS2 (pH 5.9) to give the bistability observed in our experiments at high aluminum concentrations (Figures 3b and 4b).

The BSFA model is able to reproduce small-amplitude oscillations (OSC1) (Figure 7a), MMOs with different numbers of small peaks (Figure 7b,c), and large-amplitude oscillations (OSC2) (Figure 7d).

In the computations, we replaced the nonanalytical Heaviside function $\Theta(x - K)$ by the analytical approximation

$$x^n/(x^n + K^n) \quad (15)$$

We verified that, for the exponent $n > 4$ in function 15, the difference between the numerical solutions of the BSFA model with the Heaviside function and with function 15 is numerically negligible. However, analytical function 15 allows us to analyze the stability of attractors and construct the bifurcation curves by continuation methods using the bifurcation software AUTO.[30]

As k_0 increases, small-amplitude oscillations (OSC1) emerge via supercritical Hopf bifurcation of the low-pH steady state (SS1) (Figure 8a). At higher k_0, the OSC1 regime becomes unstable, and MMOs appear. We found the following sequence of bifurcations OSC1 $\rightarrow \cdots \rightarrow M_i \rightarrow M_{i-1} \rightarrow \cdots \rightarrow M_1 \rightarrow$ OSC2 as k_0 increases, where M_i is an MMO region with one large and i small peaks. The duration of a small peak in an MMO region is roughly half that of the large peak (see Figure 7), mirroring our experimental observations (Figure 2b).

The experiments show that the small-amplitude oscillations (OSC1) can coexist with SS1 at larger $[Al^{3+}]_0$ and relatively large $[Fe(CN)_6^{4-}]_0$, as demonstrated by the narrow region of bistability between SS1 and OSC1 in Figure 3c. As noted above, OSC1 emerges via supercritical Hopf bifurcation at small k_0. Bistability between SS1 and OSC1 demonstrates that, at larger k_0, OSC1 can emerge or disappear (depending on the direction of change of k_0) through a subcritical Hopf bifurcation (at the other side of the oscillatory region). This behavior is also observed in the BSFA model at larger a_{in} and larger k_0, as well as at smaller K_p, as shown in Figure 8b. In an interval of k_0 close to 0.0035 s^{-1}, the stable steady state SS1 (pH $\approx$ 4.2) coexists with the stable limit cycle corresponding to OSC1. Figure 8b also demonstrates the bistability between SS1 and OSC2 at still larger k_0, which we did not observe in our experiments, probably because this region is so narrow.

The experiments also establish that large concentrations of aluminum ($a_{in} > 0.007$ M) kill oscillations (see, for example, Figure 3b,c). Analogous behavior is seen in Figure 8c. For large a_{in}, we observe only bistability between the low-pH steady state (SS1) and the high-pH steady state (SS2). This bistability, which occurs in a relatively small k_0 interval, is observed in the experiments as well (bistability region for $[Al^{3+}]_0 > 0.01$ M in Figure 3b).

We obtain good agreement between experiment and the model at all a_{in} only if we use different values of the constant K_p for low and high a_{in}, namely, $K_p = 4.68 \times 10^{-16}$ M^2 and $K_p = 4.68 \times 10^{-15}$ M^2, respectively. This adjustment of K_p is associated with the dependence of K_S, the solubility product

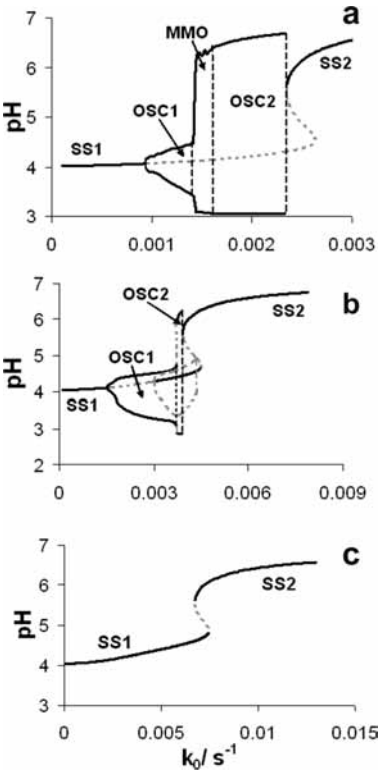

Figure 8. Bifurcation diagrams for the BSFA model. Black lines denote stable attractors (stationary states and limit cycles), and gray dotted lines denote unstable ones. Parameters: (a) As in Figure 7. (b) a_{in}= 0.005 M, $K_p = 4.68 \times 10^{-15}$ M^2, other parameters as in part a. (c) a_{in}= 0.008 M, $K_p = 4.68 \times 10^{-15}$ M^2, other parameters as in part a. Vertical dashed lines separate areas corresponding to different types of oscillations.

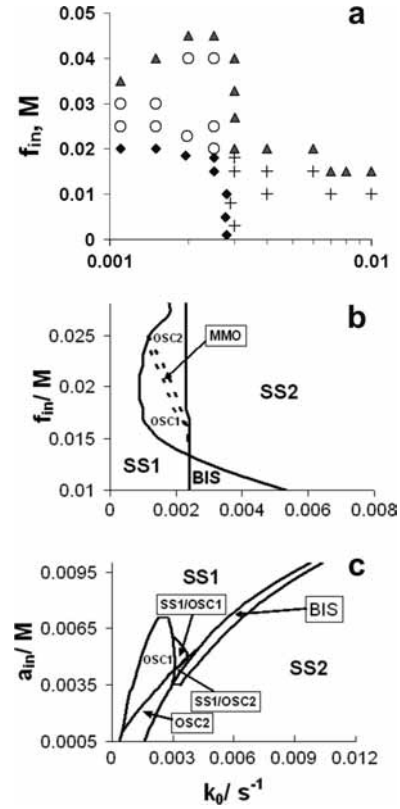

Figure 9. Parametric diagram: (a) BSF model in the k_0-f_{in} plane. Symbols: (♦) SS1 with low pH, (▲) SS2 with high pH, (+) bistability, (○) oscillatory region. Parameters as in Figure 6a. Note that the abscissa is logarithmic. Compare this figure to Figure 1a. (b) BSFA model (eqs B57−B60) in the k_0-f_{in} plane. BIS, OSC1, OSC2, SS1, and SS2 denote bistability, small-amplitude oscillation, large-amplitude oscillation, low-pH steady state, and high-pH steady state, respectively. MMOs appear in the region between the two almost parallel dotted lines. Parameters: $a_{in} = 0.0023$ M, $K_p = 4.68 \times 10^{-16}$ M^2, other parameters as in Figure 6b. (c) BSFA model in the k_0-a_{in} plane; $f_{in} = 0.022$ M, other parameters and notation as in b. Symbols SS1/OSC2 and SS1/OSC1 denote coexisting regions of the corresponding attractors.

constant of $Al(OH)_3$, and hence K_p, on the ionic strength I and, in turn, of I on a_{in}. K_S has been found to be as high as $10^{-31.6}$ M^4 for $a_{in} = 0.1$ M and as low as $10^{-33.2}$ M^4 for small a_{in}.[18,31] We obtained good agreement between experiment and the model when we used $K_S = 10^{-33.2}$ for small a_{in} ($a_{in} < 0.007$ M) and $K_S = 10^{-32.2}$ for large a_{in} ($a_{in} > 0.007$ M).

To test the BSF and BSFA models, we compared their dynamic behavior in the k_0-f_{in} and k_0-a_{in} planes with our experimental results. The calculated k_0-f_{in} phase diagram showing the regions of oscillation and bistability for the BSF model (Figure 9a) coincides well with the experimentally found diagram in Figure 1a. The k_0-f_{in} phase diagram for the BSFA model (Figure 9b) shows qualitative agreement between the model and experiment (Figure 3a). The boundaries between the SS and oscillatory regions were found by linear stability analysis of the SSs of the BSFA model, whereas the boundaries between the different types of oscillatory behavior were obtained by direct numerical integration of the BSFA model. Note also the similarity between the analogous diagrams in the k_0-f_{in} plane for the BSF model (Figure 9a) and the BSFA model (Figure 9b). The main difference between these two is that the oscillatory region in Figure 9b is split into three subregions: OSC1, MMO, and OSC2.

The dynamic behavior of the BSFA model in the k_0-a_{in} plane (Figure 9c) shows qualitative agreement with the experimental results (Figure 3b) as well. This parametric diagram was constructed using $K_p = 4.68 \times 10^{-16}$ M^2 for $a_{in} \leq 0.0023$ M, $K_p = 4.68 \times 10^{-15}$ M^2 for $a_{in} \geq 0.008$ M, and a linear dependence of K_p on a_{in} in the interval $a_{in} \in$ (0.0023 M, 0.008 M). All of the important features of the experimental system are reproduced: narrow domains of oscillation and bistability, small-amplitude (OSC1) and large-amplitude (OSC2) oscillations, and coexistence of SS1 and OSC1 (see Figure 8b). However, all of these domains appear at k_0 values smaller than in the experiments. The main difference between the experiments (Figure 3a) and the model (Figure 9c) occurs in the region $[Al^{3+}]_0 \in$ (0.004 M, 0.008 M) in Figure 3a. In the experiments, we have only OSC2, SS2, and bistablity SS1/SS2 for $[Al^{3+}]_0$= 0.0045 M, 0.007, and 0.01 M, respectively. In the BSFA model, the situation is more complicated. We find bistability between SS1 and OSC1 (SS1/OSC1) and between SS1 and OSC2 (SS1/OSC2) for $a_{in} \in$ (0.004 M, 0.0065 M) in Figure 9c. We should probably not expect more quantitative agreement with our simple BSFA model, because the reversible process of precipitation has been incorporated into the model in an oversimplified manner through the Heaviside function without taking into account the different forms and sizes of the precipitated particles.

Discussion and Conclusion

Our experimental results demonstrate that novel pH oscillations, namely, small-amplitude and mixed-mode oscillations, can be generated by coupling a well-characterized pH oscillator, the BSF system, to a precipitation equilibrium, reaction 1 with Al^{3+}. We have constructed a two-variable model for the BSF system and augmented it with a simple description of the

precipitation equilibrium to yield the four-variable BSFA model that qualitatively reproduces all of our experimental findings. The development of a simple model and experimental characterization of the dynamic behavior of the BSFA system (e.g., the phase diagrams in Figure 3) were the main goals of this work. However, the discovery of MMOs raises additional questions about the origin of MMOs, which we address here very briefly.

There have been many studies of mixed-mode oscillations.[32−45] MMOs are found in electrochemical systems[32,41,44,45] and in chemical systems such as the Belousov−Zhabotinsky reaction,[33,46] the peroxidase−oxidase enzymatic reaction,[40,47] the chlorine dioxide−iodide reaction,[48] and others. In all cases, a description of MMOs requires three or more variables. Because the majority of pH oscillators can be satisfactorily described by two variables, the proton (h) and substrate (s) concentrations, as in the BSF model, MMOs are a rare phenomenon among pH oscillators. MMOs have been found in the BSF system under illumination[27] and in the $SO_3^{-}-H_2O_2-$marble system.[49] The $Al(OH)_3(s)$ precipitate in the BSF system and the marble in the $SO_3^{-}-H_2O_2$ system are analogous: both consist of solid particles that play the role of the crucial third independent variable. However, there are obvious differences as well. For example, in the latter system, the marble only dissolves, whereas in the former system, $Al(OH)_3$ precipitation is reversible.

MMOs can originate via several dynamical scenarios: a homoclinic orbit around a saddle focus resulting from the interaction of a fast two-dimensional oscillatory subsystem with a one-dimensional slow S-shaped manifold, a canard expolosion, a Shil'nikov homoclinic loop, a period-doubling cascade, a period-adding regime, or chaotic oscillations.[32,41,43−45] MMOs can also give rise to Farey sequences,[50] although we did not observe that phenomenon in this system. These theoretical questions lie beyond the scope of the present work. Here, using the BSFA model, we simply take a deeper look at the role played by the $Al(OH)_3$ precipitate in the emergence of these complex oscillations.

Reactions 2 and 3 always produce protons, and reaction 4 together with equilibrium 11 consumes protons, but the roles of reactions 5 and 6, responsible for precipitation−dissolution, and reaction 13 are not so straightforward. We can analyze the contribution of these reactions to the rate dh/dt using eq B58 and the steady-state value, h_{SS}, calculated numerically for the oscillatory region. At these parameters, pH_{SS} lies between 4.1 and 4.2. The term $(r_5 - r_6)$ changes sign in the pH range 3.9−4.1 (different values of pH correspond to different phases of the oscillation) for small-amplitude oscillations and in the pH range 3.9−4.3 for large-amplitude oscillations, always being negative at pH < 3.9 and positive at pH > 4.3. Thus, the term $(r_5 - r_6)$ always forces the system toward the SS, manifesting itself as a stabilizing negative feedback. Although Al^{3+} works as a negative feedback, the rate $(r_5 - r_6)$ at pH < 3.8 is much smaller than the more powerful negative feedback of rate r_4. Therefore, addition of Al^{3+} to the $BrO_3^{-}-SO_3^{2-}$ subsystem without $Fe(CN)_6^{4-}$ is not sufficient to produce oscillatory behavior.

The term $(1 - D_S)$, which multiplies r_{13} in eq B58, also changes sign at pH values close to pH_{SS}, at $h_S = (K_{S1}K_{S2})^{-1/2}$ ($pH_S \approx 4.4$), being negative at $h < h_S$ and positive otherwise. Therefore reaction 13 serves as negative feedback when $pH < pH_{SS}$ and $pH > pH_S > pH_{SS}$, whereas between pH_S and pH_{SS}, reaction 13 destabilizes the steady state.

We also analyzed the signs of the Jacobian matrix, $\mathbf{J}(s,h,p,m)$, at the steady states, i.e., the community matrix,[51] for parameters corresponding to the oscillatory region (as in Figure 8, for example), varying only k_0 in such a way that the system exhibits small-amplitude oscillations, MMOs, and large-amplitude oscillations.

$$\mathrm{sign}[\mathbf{J}(s,h,p,m)_{SS}] = \begin{pmatrix} - & - & + & + \\ + & + & \pm & + \\ 0 & - & - & 0 \\ + & + & - & - \end{pmatrix} \qquad (16)$$

The matrix in eq 16 shows that only species h is autocatalytic, because only one diagonal element, J_{22} ($\equiv J_{hh}$), is positive. Element J_{23} ($\equiv J_{hp}$) changes sign from positive to negative as the system moves from MMOs to large-amplitude oscillations (k_0 increases). This observation suggests that positive J_{23} might be important for MMOs (as well as for small-amplitude oscillations).

To clarify this notion, we explore the possibility of indirect or cross-autocatalysis.[51] For example, elements J_{41} and J_{14} create a positive feedback through cross-autocatalysis, because both sign(J_{41}) and sign(J_{14}) are positive. An increase in s leads to an increase in dm/dt ($J_{41} > 0$), resulting in an increase in m; in turn, an increase in m leads to an increase in ds/dt ($J_{14} > 0$) and, consequently, to an increase in s. Positive elements J_{42} and J_{24} also indicate cross-autocatalysis between h and m, underlining the key role of m. In general, a positive feedback can be created whenever two elements J_{ij} and J_{ji} have the same sign. Indeed, an increase in h leads to a decrease in dp/dt ($J_{32} < 0$). If this decrease is so strong that dp/dt becomes negative and leads to a decrease in p, then this decrease in p results in an increase in dh/dt ($J_{23} < 0$), which can lead to positive feedback. The rate dp/dt can change sign in the vicinity of the SS, because dp/dt depends strongly on the sign of $(r_5 - r_6)$ (see eq B59), which, as noted above, changes in the pH range 3.9−4.3.

In our case, the MMOs are embedded between simple periodic limit cycles when a bifurcation parameter (for example, k_0) is changed. Therefore, the transition to the MMO regime might arise from a bifurcation of a limit cycle, rather than from a change in the character of the steady state, and the Jacobian matrix would then offer little help in explaining the MMOs. We note, however, that MMOs can also result from interaction between a pair of limit cycles, as in the case of two coupled chemical oscillators.[48] The abrupt transition from small- to large-amplitude oscillations known as a canard explosion[52] can also be associated with MMOs.[53] The canard phenomenon signals the existence of two different limit cycles that can sometimes coexist at the same value of the bifurcation parameter. In our system, there are two limit cycles, OSC1 and OSC2. The emergence of one (or both) of these can occur in the parameter range of the MMOs and can originate from the change in sign of the Jacobian matrix element, J_{23}. Roughly speaking, OSC1 is created by the BSFA system and is stable at lower values of k_0, while OSC2 is created by the BSF subsystem and is stable at higher k_0. For intermediate k_0 values, both simple limit cycles are unstable. More detailed analysis is necessary to fully elucidate the origin of MMOs in the BSFA system.

Our experimental results suggest the possibility that coupling other pH-oscillatory systems to appropriate precipitation equilibria can generate new pH oscillators and complex oscillations. The new four-variable BSFA model also makes it possible to better understand the mechanism and the dynamical behavior of such coupled systems.

Acknowledgment. This work was supported by the National Science Foundation under Grant CHE-0615507.

Appendix A. Two-Variable BSF Model

The chemical reactions for the $BrO_3^- - SO_3^{2-} - Fe(CN)_6^{4-}$ system can be written as

$$3s_1 + b \rightarrow 3h + 3m_0 \quad r_2 = k_2 s_1 b \tag{A1}$$

$$3s_2 + b \rightarrow 6h + 3m_0 \quad r_3 = k_3 s_2 b \tag{A2}$$

$$6f_1 + b \rightarrow 0 \quad r_4 = k_4 f_1 b \tag{A3}$$

$$s_0 + h \rightleftarrows s_1 \quad K_{S1} \tag{A4}$$

$$s_1 + h \rightleftarrows s_2 \quad K_{S2} \tag{A5}$$

$$m_0 + h \rightleftarrows m_1 \quad K_{SA} \tag{A6}$$

$$f_0 + h \rightleftarrows f_1 \quad K_F \tag{A7}$$

$$o + h \rightleftarrows H_2O \quad K_w \tag{A8}$$

where $s_0 = [SO_3^{2-}]$, $s_1 = [HSO_3^-]$, $s_2 = [H_2SO_3]$, $b = [BrO_3^-]$, $f_0 = [Fe(CN)_6^{4-}]$, $f_1 = [HFe(CN)_6^{3-}]$, $o = [OH^-]$, $h = [H^+]$, $m_0 = [SO_4^{2-}]$, and $m_1 = [HSO_4^-]$. We omit the rather slow reaction 13 in Table 1.

The reaction rates are expressed by the following ODEs

$$ds_0/dt = k_0(s_{in} - s_0) - R_8 \tag{A9}$$

$$ds_1/dt = -k_0 s_1 + R_8 - R_9 - 3r_2 \tag{A10}$$

$$ds_2/dt = -k_0 s_2 + R_9 - 3r_3 \tag{A11}$$

$$df_0/dt = k_0(f_{in} - f_0) - R_{11} \tag{A12}$$

$$df_1/dt = -k_0 f_1 + R_{11} - 6r_4 \tag{A13}$$

$$db/dt = k_0(b_{in} - b) - r_2 - r_3 - r_4 \tag{A14}$$

$$dh/dt = k_0(h_{in} - h) - R_8 - R_9 - R_{10} - R_{11} - R_{12} + 3r_2 + 6r_3 \tag{A15}$$

$$do/dt = -k_0 o - R_{12} \tag{A16}$$

$$dm_0/dt = k_0(m_{in} - m_0) - R_{10} + 3r_2 + 3r_3 \tag{A17}$$

$$dm_1/dt = -k_0 m_1 + R_{10} \tag{A18}$$

where $R_8 = k_d(s_0 h - s_1/K_{S1})$, $R_9 = k_d(s_1 h - s_2/K_{S2})$, $R_{10} = k_d(m_0 h - m_1/K_{SA})$, $R_{11} = k_d(f_0 h - f_1/K_F)$, $R_{12} = k_d(oh - 1/K_w)$, and k_d is the diffusion-controlled reaction rate constant; the subscript "in" denotes input concentrations of reactants ($m_{in} = [H_2SO_4]_{in} = h_{in}/2$), and k_0^{-1} is the residence time.

Using the mass balance relations

$$s \equiv s_0 + s_1 + s_2 \tag{A19}$$

$$f_t \equiv f_0 + f_1 \tag{A20}$$

$$m \equiv m_0 + m_1 \tag{A21}$$

and fast equilibrium reactions 8−11 shown in Table 1, we can express the variables s_1, s_2, f_1, m_1, and o (as well as s_0, f_0, and m_0) in terms of s, f_t, m, and h as

$$s_1 = sD_{S1} \tag{A22}$$

$$s_2 = sD_{S2} \tag{A23}$$

$$f_1 = f_t D_F \tag{A24}$$

$$m_1 = mD_m \tag{A25}$$

$$o = 1/hK_w \tag{A26}$$

where

$$D_{S1} = K_{S1}h/(1 + K_{S1}h + K_{S1}K_{S2}h^2) \tag{A27}$$

$$D_{S2} = K_{S1}K_{S2}h^2/(1 + K_{S1}h + K_{S1}K_{S2}h^2) \tag{A28}$$

$$D_F = K_F h/(1 + K_F h) \tag{A29}$$

$$D_m = K_{SA}h/(1 + K_{SA}h) \tag{A30}$$

Combining eqs A9−A18 and using relations A22−A26, we can eliminate fast equilibrium reactions included in term R_8, R_9, R_{10}, R_{11}, and R_{12}. Summation of eqs A9−A11 and use of eq A19 gives

$$ds/dt = k_0(s_{in} - s) - 3r_2 - 3r_3 \tag{A31}$$

Summation of eqs A12 and A13 together with eq A20 gives

$$df_t/dt = k_0(f_{in} - f_t) - 6r_4 \tag{A32}$$

Summation of eqs A17 and A18 using eq A21 gives

$$dm/dt = k_0(m_{in} - m) + 3r_2 + 3r_3 \tag{A33}$$

Summing $s_1 + 2s_2 + f_1 + m_1 + h - o$ and substituting eqs A22−A26, we can write the identity

$$s_1 + 2s_2 + f_1 + m_1 + h - o = sD_S + f_t D_F + mD_m + h - 1/hK_w \tag{A34}$$

where $D_S = D_{S1} + 2D_{S2}$. Differentiation of the identity in eq A34 with respect to time gives

$$d(s_1 + 2s_2 + f_1 + m_1 + h - o)/dt = (dh/dt)D + (ds/dt)D_S + (df_t/dt)D_F + (dm/dt)D_m \tag{A35}$$

where $D = D(s,f_t,m,h) = [K_{S1}s(1 + 4K_{S2}h + K_{S1}K_{S2}h^2)/(1 + K_{S1}h + K_{S1}K_{S2}h^2)^2 + f_t K_F/(1 + K_F h)^2 + mK_{SA}/(1 + K_{SA}h)^2 + 1 + 1/h^2K_w]$. Substituting eqs A10, A11, A13, A15, A16, and A18 into the left-hand side of eq A35 and eqs A31−A33 into the right-hand side, we have

$$(dh/dt)D = k_0(-s_{in}D_S - f_{in}D_F - m_{in}D_m + sD_S + f_t D_F + mD_m - f_t + f_{in}) + 3(r_2 + r_3)(D_S - D_m) - 6r_4(1 - D_F) \tag{A36}$$

Summation of eqs A31 and A33 gives

$$d(s + m)/dt = k_0(s_{in} - s + m_{in} - m) \tag{A37}$$

and, consequently, at long times (when $t \gg k_0^{-1}$)

$$m = s_{in} + m_{in} - s \tag{A38}$$

Note that the condition $t \gg k_0^{-1}$ is practically fullfiled after two to three periods of oscillations.

Combining 6(eq A14) + 2(eq A33) − (eq A32), we have

$$d(6b + 2m - f_t)/dt = k_0(6b_{in} - 6b + 2m_{in} - 2m - f_{in} + f_t) \tag{A39}$$

Using eq A38 and assuming long times ($t \gg k_0^{-1}$), we get from eq A39

$$b = b_{in} - f_{in}/6 - s_{in}/3 + f_t/6 + s/3 \tag{A40}$$

Summation of (eq A10) + 2(eq A11) + (eq A13) + (eq A18) + (eq A15) − (eq A16) − (eq A32) gives

$$d(s_1 + 2s_2 + f_1 + m_1 + h - o - f_t)/dt = k_0(h_{in} - f_{in} - s_1 - 2s_2 - f_1 - m_1 - h + o + f_t) \tag{A41}$$

and, consequently, at long times ($t \gg k_0^{-1}$)

$$s_1+2s_2+f_1+m_1+h-o-f_t=h_{in}-f_{in} \quad \text{(A42)}$$

Using eqs A22−A26, eq A42 yields

$$sD_S+f_tD_F+mD_m-f_t+f_{in}=h_{in}-h+1/hK_w \quad \text{(A43)}$$

or

$$f_t=[s(D_S-D_m)+(s_{in}D_m+m_{in}D_m+f_{in}-h_{in}+h-h^{-1}K_w{}^{-1})](1+K_Fh) \quad \text{(A43m)}$$

Substituting eq A43 into eq A36 and eliminating m, b, and f_t, using eqs A38, A40, and A43m, respectively, we finally have a two-variable BSF model

$$ds/dt=k_0(s_{in}-s)-3(r_2+r_3) \quad \text{(A44)}$$

$$dh/dt=[k_0H_h+3(r_2+r_3)(D_S-D_m)-6r_4(1-D_F)]/D \quad \text{(A45)}$$

where $H_h \equiv (h_{in}-h+h^{-1}K_w{}^{-1}-s_{in}D_S-f_{in}D_F-m_{in}D_m)$, $r_2+r_3=B(s,h)shK_{S1}[(k_2+k_3K_{S2}h)/(1+K_{S1}h+K_{S1}K_{S2}h^2)]$, $r_4=k_4D_FF(s,h)B(s,h)$, $F(s,h)\equiv f_t$ is given by eq A43m, $B(s,h)\equiv b$ is given by eq A40, and $D\equiv D(s,h)=[sD_{Sd}+F(s,h)K_F/(1+K_Fh)^2+(s_{in}+m_{in}-s)K_{SA}/(1+K_{SA}h)^2+1+1/(h^2K_w)]$, $D_{Sd}=K_{S1}(1+4K_{S2}h+K_{S1}K_{S2}h^2)/(1+K_{S1}h+K_{S1}K_{S2}h^2)^2$. Note that $D_S > D_m$ at any h for the constants K_{S1}, K_{S2}, and K_{SA} used here, and consequently, the term (D_S-D_m) in the numerator of eq A45 is positive. The term $(1-D_F)=1/(1+K_Fh)$ is also positive. The terms $h^{-1}K_w{}^{-1}$ and $1/(h^2K_w)$ are very small and can be omitted if pH < 7.

Appendix B. Deduction of a Model for the BrO_3^-−SO_3^{2-}−$Fe(CN)_6^{4-}$−Al^{3+} (BSFA) System

The chemical reactions for the BSFA system can be written as

$$3s_1+b\rightarrow 3h+3m_0 \qquad r_2=k_2s_1b \quad \text{(B1)}$$

$$3s_2+b\rightarrow 6h+3m_0 \qquad r_3=k_3s_2b \quad \text{(B2)}$$

$$6f_1+b\rightarrow 0 \qquad r_4=k_4f_1b \quad \text{(B3)}$$

$$a_2+o\rightarrow p \qquad r_5=k_5a_2o\times\Theta(a_2o-K_p) \quad \text{(B4)}$$

$$p\rightarrow a_2+o \qquad r_6=k_6\times\Theta(p) \quad \text{(B5)}$$

$$a_0+2o\rightleftarrows a_2 \qquad K_A \quad \text{(B6)}$$

$$s_0+h\rightleftarrows s_1 \qquad K_{S1} \quad \text{(B7)}$$

$$s_1+h\rightleftarrows s_2 \qquad K_{S2} \quad \text{(B8)}$$

$$m_0+h\rightleftarrows m_1 \qquad K_{SA} \quad \text{(B9)}$$

$$f_0+h\rightleftarrows f_1 \qquad K_F \quad \text{(B10)}$$

$$o+h\rightleftarrows H_2O \qquad K_w \quad \text{(B11)}$$

$$6s_2+b\rightarrow 6h \qquad r_{13}=k_{13}s_2b \quad \text{(B12)}$$

where $\Theta(x)=0$ if $x<0$ and $\Theta(x)=1$ if $x>0$, $s_0=[SO_3^{2-}]$, $s_1=[HSO_3^-]$, $s_2=[H_2SO_3]$, $b=[BrO_3^-]$, $f_0=[Fe(CN)_6^{4-}]$, $f_1=[HFe(CN)_6^{3-}]$, $o=[OH^-]$, $h=[H^+]$, $a_0=[Al^{3+}]$, $a_2=[Al(OH)_2^+]$, $p=[Al(OH)_{3(s)}]$, $m_0=[SO_4^{2-}]$, and $m_1=[HSO_4^-]$,

The reaction rates are expressed by the following ODEs

$$ds_0/dt=k_0(s_{in}-s_0)-R_8 \quad \text{(B13)}$$

$$ds_1/dt=-k_0s_1+R_8-R_9-3r_2 \quad \text{(B14)}$$

$$ds_2/dt=-k_0s_2+R_9-3r_3-6r_{13} \quad \text{(B15)}$$

$$df_0/dt=k_0(f_{in}-f_0)-R_{11} \quad \text{(B16)}$$

$$df_1/dt=-k_0f_1+R_{11}-6r_4 \quad \text{(B17)}$$

$$db/dt=k_0(b_{in}-b)-r_2-r_3-r_4-r_{13} \quad \text{(B18)}$$

$$da_0/dt=k_0(a_{in}-a_0)-R_7 \quad \text{(B19)}$$

$$da_2/dt=-k_0a_2+R_7-r_5+r_6 \quad \text{(B20)}$$

$$dp/dt=-k_0p+r_5-r_6 \quad \text{(B21)}$$

$$dh/dt=k_0(h_{in}-h)-R_8-R_9-R_{10}-R_{11}-R_{12}+3r_2+6r_3+6r_{13} \quad \text{(B22)}$$

$$do/dt=-k_0o-2R_7-r_5+r_6-R_{12} \quad \text{(B23)}$$

$$dm_0/dt=k_0(m_{in}-m_0)-R_{10}+3r_2+3r_3 \quad \text{(B24)}$$

$$dm_1/dt=-k_0m_1+R_{10} \quad \text{(B25)}$$

where $R_7=k_d'(a_0o^2-a_2/K_A)$; $R_8=k_d(s_0h-s_1/K_{S1})$; $R_9=k_d(s_1h-s_2/K_{S2})$; $R_{10}=k_d(m_0h-m_1/K_{SA})$; $R_{11}=k_d(f_0h-f_1/K_F)$; $R_{12}=k_d(oh-1/K_w)$; k_d and k_d' are the diffusion-controlled reaction rate constants for bimolecular and trimolecular reactions, respectively; the subscript "in" denotes input concentrations of reactants; and $k_0{}^{-1}$ is the residence time.

The system of eqs B13−B25 can be simplified using the mass balance relations

$$s\equiv s_0+s_1+s_2 \quad \text{(B26)}$$

$$f\equiv f_0+f_1 \quad \text{(B27)}$$

$$m\equiv m_0+m_1 \quad \text{(B28)}$$

$$a\equiv a_0+a_2 \quad \text{(B29)}$$

$$h_t=h+s_1+2s_2+f_1+m_1 \quad \text{(B30)}$$

$$o_t=o+2a_2 \quad \text{(B31)}$$

Summation of eqs B13−B15 gives

$$ds/dt=k_0(s_{in}-s)-3_{r2}-3_{r3}-6r_{13} \quad \text{(B32)}$$

Summation of eqs B16 and B17 gives

$$df/dt=k_0(f_{in}-f)-6r_4 \quad \text{(B33)}$$

Summation of eqs B19 and B20 gives

$$da/dt=k_0(a_{in}-a)-r_5+r_6 \quad \text{(B34)}$$

Summation of eqs B24 and B25 gives

$$dm/dt=k_0(m_{in}-m)+3r_2+3r_3 \quad \text{(B35)}$$

Summation of (eq B14) + 2(eq B15) + (eq B17) + (eq B22) + (eq B25) gives

$$dh_t/dt=k_0(h_{in}-h_t)-6r_4-R_{12}-6r_{13} \quad \text{(B36)}$$

Summation of (eq B23) + 2(eq B20) gives

$$do_t/dt=-k_0o_t-3r_5+3r_6-R_{12} \quad \text{(B37)}$$

Finally, subtraction of eq B37 from eq B36 gives

$$d(h_t-o_t)/dt=k_0(h_{in}-h_t+o_t)-6r_4+3r_5-3r_6-6r_{13} \quad \text{(B38)}$$

Using the fact that equilibrium reactions 7−12 are very fast, reaction rates r_2, r_3, r_4, r_5, and r_{13} can now be expressed in terms of the variables s, f, a, and h. Because of the equilibria, we can write

$$s_1=K_{S1}s_0h \quad \text{(B39)}$$

$$s_2=K_{S1}K_{S2}s_0h^2 \quad \text{(B40)}$$

$$f_1 = K_F f_0 h \quad \text{(B41)}$$

$$m_1 = K_{SA} m_0 h \quad \text{(B42)}$$

$$a_2 = K_A a_0 o^2 \quad \text{(B43)}$$

$$K_w o h = 1 \quad \text{(B44)}$$

which allows the reaction rates, r_i, to be rewritten as

$$r_2 = k_2 b s h K_{S1}/(1 + K_{S1}h + K_{S1}K_{S2}h^2) \quad \text{(B45)}$$

$$r_3 = k_3 b s K_{S1}K_{S2}h^2/(1 + K_{S1}h + K_{S1}K_{S2}h^2) \quad \text{(B46)}$$

$$r_4 = k_4 b f h K_F/(1 + K_F h) \quad \text{(B47)}$$

$$r_5 = k_5 a K_A o^3/(1 + K_A o^2) \times \Theta[a K_A o^3/(1 + K_A o^2) - K_p] \quad \text{(B48)}$$

$$r_{13} = k_{13} b s K_{S1}K_{S2}h^2/(1 + K_{S1}h + K_{S1}K_{S2}h^2) \quad \text{(B49)}$$

where o in eq B48 is equal to $1/hK_w$.

Now we express $(h_t - o_t)$ in eq B38 in terms of h, s, f, a, and m. From eqs B30 and B31, it follows that

$$h_t - o_t = h + s_1 + 2s_2 + f_1 + m_1 - o - 2a_2 = h - 1/hK_w + sK_{S1}h(1 + 2K_{S2}h)/(1 + K_{S1}h + K_{S1}K_{S2}h^2) + fK_F h/(1 + K_F h) + mK_{SA}h/(1 + K_{SA}h) - 2aK_A/(h^2K_w{}^2 + K_A) \quad \text{(B50)}$$

Next, we differentiate eq B50 with respect to time to obtain

$$\mathrm{d}(h_t - o_t)/\mathrm{d}t = D\mathrm{d}h/\mathrm{d}t + D_S\mathrm{d}s/\mathrm{d}t + D_F\mathrm{d}f/\mathrm{d}t + D_m\mathrm{d}m/\mathrm{d}t - D_a\mathrm{d}a/\mathrm{d}t \quad \text{(B51)}$$

where $D(h,s,f,m,a) \equiv D = 1 + 1/(h^2K_w) + sK_{S1}(1 + 4hK_{S2} + K_{S1}K_{S2}h^2)/(1 + K_{S1}h + K_{S1}K_{S2}h^2)^2 + f_tK_F/(1 + K_F h)^2 + mK_{SA}/(1 + K_{SA}h)^2 + 4ahK_AK_w{}^2/(h^2K_w{}^2 + K_A)^2$, $D_S = K_{S1}h(1 + 2K_{S2}h)/(1 + K_{S1}h + K_{S1}K_{S2}h^2)$, $D_F = K_F h/(1 + K_F h)$, $D_m = K_{SA}h/(1 + K_{SA}h)$, and $D_a = 2K_A/(h^2K_w{}^2 + K_A)$.

Substituting expressions for $\mathrm{d}s/\mathrm{d}t$ from eq B32, for $\mathrm{d}f/\mathrm{d}t$ from eq B33, for $\mathrm{d}a/\mathrm{d}t$ from eq B34, and for $\mathrm{d}m/\mathrm{d}t$ from eq B35 into into eq B51, substituting the result into eq B38, and regrouping gives an expression for $\mathrm{d}h/\mathrm{d}t$ as

$$D\mathrm{d}h/\mathrm{d}t = k_0(h_{in} - D_S s_{in} - D_F f_{in} - D_m m_{in} + D_a a_{in} - h + 1/hK_w) + 3(D_S - D_m)(r_2 + r_3) - 6(1 - D_S)r_{13} - 6(1 - D_F)r_4 + (3 - D_a)(r_5 - r_6) \quad \text{(B52)}$$

Equation B52 together with eqs B18, B21, and B32−B35 constitute a set of equations for the seven variables h, s, f, b, a, p, and m that does not contain the fast equilibrium reactions.

Further simplifications can be made. Summing eqs B34 and B21, it follows that $\mathrm{d}(p + a)/\mathrm{d}t = k_0(a_{in} - a - p)$. This gives (at $t \gg k_0^{-1}$)

$$a_{in} = a + p \quad \text{(B53)}$$

Combination of 6(eq B18) − (eq B32) + (eq B35) + (eq B33) gives $\mathrm{d}(6b - s + m - f)/\mathrm{d}t = k_0(6b_{in} - s_{in} + m_{in} - f_{in} - 6b + s - m + f)$, which implies (at $t \gg k_0^{-1}$) that

$$b = b_{in} - (s_{in} - m_{in} + f_{in} - s + m - f)/6 \quad \text{(B54)}$$

Combining (eq B38) − (eq B32) − (eq B35) − (eq B33) − 3(eq B21), we obtain

$$\mathrm{d}(h + s_2 - s_0 - f_0 - o - 2a_2 - 3p - m_0)/\mathrm{d}t = k_0(h_{in} - s_{in} - m_{in} + f_{in} - h - s_2 + s_0 + f_0 + o + 2a_2 + 3p + m_0)$$

which gives (at $t \gg k_0^{-1}$)

$$f_0 = h + s_2 - s_0 - m_0 - o - 2a_2 - 3p - h_{in} + s_{in} + m_{in} + f_{in} \quad \text{(B55)}$$

Using the relations

$$s_1 = sK_{S1}h/(1 + K_{S1}h + K_{S1}K_{S2}h^2)$$

$$s_2 = sK_{S1}K_{S2}h^2/(1 + K_{S1}h + K_{S1}K_{S2}h^2)$$

$$m_1 = mK_{SA}h/(1 + K_{SA}h)$$

$$o = 1/hK_w$$

$$a_2 = aK_A/(h^2K_w{}^2 + K_A) = (a_{in} - p)K_A/(h^2K_w{}^2 + K_A)$$

$$f_0 = f/(1 + K_F h)$$

from eq B55, we can express f as a function of h, p, s, and m as

$$F(h,p,s,m) = (1 + K_F h)[h + s(K_{S1}K_{S2}h^2 - 1)/(1 + K_{S1}h + K_{S1}K_{S2}h^2) - m/(1 + K_{SA}h) - 1/hK_w - 2(a_{in} - p)K_A/(h^2K_w{}^2 + K_A) - 3p - h_{in} + s_{in} + m_{in} + f_{in}] \quad \text{(B56)}$$

Equations B54−B56 allow for the elimination of three variables, for example, a, b, and f, substituting $a = a_{in} - p$, $b = b_{in} - [s_{in} - m_{in} + f_{in} - s + m - F(h,p,s,m)]/6$, and $f = F(h,p,s,m)$ into the expressions for rates r_i and D. Finally, we have a system of four differential equations

$$\mathrm{d}s/\mathrm{d}t = k_0(s_{in} - s) - 3r_2 - 3r_3 - 6r_{13} \quad \text{(B57)}$$

$$D\mathrm{d}h/\mathrm{d}t = k_0(h_{in} - D_S s_{in} - D_F f_{in} - D_m m_{in} + D_a a_{in} - h + 1/hK_w) + 3(D_S - D_m)(r_2 + r_3) - 6r_{13}(1 - D_S) - 6r_4/(1 + K_F h) + (3 - D_a)(r_5 - r_6) \quad \text{(B58)}$$

$$\mathrm{d}p/\mathrm{d}t = -k_0 p + r_5 - r_6 \quad \text{(B59)}$$

$$\mathrm{d}m/\mathrm{d}t = k_0(m_{in} - m) + 3r_2 + 3r_3 \quad \text{(B60)}$$

where

$$r_2 = k_2\{b_{in} - [s_{in} - m_{in} + f_{in} - s + m - F(h,p,s,m)]/6\} s h K_{S1}/(1 + K_{S1}h + K_{S1}K_{S2}h^2) \quad \text{(B61)}$$

$$r_3 = k_3\{b_{in} - [s_{in} - m_{in} + f_{in} - s + m - F(h,p,s,m)]/6\} s K_{S1}K_{S2}h^2/(1 + K_{S1}h + K_{S1}K_{S2}h^2) \quad \text{(B62)}$$

$$r_4 = k_4\{b_{in} - [s_{in} - m_{in} + f_{in} - s + m - F(h,p,s,m)]/6\} F(h,p,s,m) h K_F/(1 + K_F h) \quad \text{(B63)}$$

$$r_5 = k_5(a_{in} - p)D_5 \times \Theta[(a_{in} - p)D_5 - K_p] \quad \text{(B64)}$$

$$r_6 = k_6 \times \Theta(p) \quad \text{(B65)}$$

$$r_{13} = k_{13}\{b_{in} - [s_{in} - m_{in} + f_{in} - s + m - F(h,p,s,m)]/6\} s K_{S1}K_{S2}h^2/(1 + K_{S1}h + K_{S1}K_{S2}h^2) \quad \text{(B66)}$$

with $D_5 = K_A/[(hK_w)^3(1 + K_A/(hK_w)^2)]$; $D = 1 + 1/(h^2K_w) + sK_{S1}(1 + 4hK_{S2} + K_{S1}K_{S2}h^2)/(1 + K_{S1}h + K_{S1}K_{S2}h^2)^2 + F(h,p,s,m)K_F/(1 + K_F h)^2 + mK_{SA}/(1 + K_{SA}h)^2 + 4(a_{in} - p)hK_AK_w{}^2/(h^2K_w{}^2 + K_A)^2$; and D_S, D_m, D_F, and D_a as before: $D_S = K_{S1}h(1 + 2K_{S2}h)/(1 + K_{S1}h + K_{S1}K_{S2}h^2)$, $D_F = K_F h/(1 + K_F h)$, $D_m = K_{SA}h/(1 + K_{SA}h)$, and $D_a = 2K_A/(h^2K_w{}^2 + K_A)$.

Note that $(3 - D_a) \geq 1$ and $(D_S - D_m) > 0$ in eq B59 at any pH. The term $(1 - D_S)$ is negative if $h^2 > 1/(K_{S1}K_{S2})$ and positive otherwise. For the K_{S1} and K_{S2} values used (see Table 1), this condition corresponds to pH 4.4.

References and Notes

(1) Luo, Y.; Epstein, I. R. *J. Am. Chem. Soc.* **1991**, *113*, 1518–1522.
(2) Howse, J. R.; Topham, P.; Crook, C. J.; Gleeson, A. J.; Bras, W.; Jones, R. A. L.; Ryan, A. J. *Nano Lett.* **2006**, *6*, 73–77.
(3) Yoshida, R.; Ichijo, H.; Hakuta, T.; Yamaguchi, T. *Macromol. Rapid Commun.* **1995**, *16*, 305–310.
(4) Yoshida, R.; Tanaka, M.; Onodera, S.; Yamaguchi, T.; Kokufuta, E. *J. Phys. Chem. A* **2000**, *104*, 7549–7555.
(5) Misra, G. P.; Siegel, R. A. *J. Controlled Release* **2002**, *79*, 293–297.
(6) Liedl, T.; Simmel, F. C. *Nano Lett.* **2005**, *5*, 1894–1898.
(7) Liedl, T.; Sobey, T. L.; Simmel, F. C. *Nano Today* **2007**, *2*, 36–41.
(8) Haim, D.; Li, G.; Ouyang, Q.; McCormick, W. D.; Swinney, H. L.; Hagberg, A.; Meron, E. *Phys. Rev. Lett.* **1996**, *77*, 190–193.
(9) Li, G.; Ouyang, Q.; Swinney, H. L. *J. Chem. Phys.* **1996**, *105*, 10830–10837.
(10) Lee, K. J.; McCormick, W. D.; Pearson, J. E.; Swinney, H. L. *Nature* **1994**, *369*, 215–218.
(11) Lee, K. J.; Swinney, H. L. *Int. J. Bifurcation Chaos* **1997**, *7*, 1149–1158.
(12) Reynolds, W. N.; Ponce-Dawson, S.; Pearson, J. E. *Phys. Rev. E* **1997**, *56*, 185–198.
(13) Lee, K. J.; Swinney, H. L. *Phys. Rev. E* **1995**, *51*, 1899–1915.
(14) Kurin-Csörgei, K.; Epstein, I. R.; Orbán, M. *Nature* **2005**, *433*, 139–142.
(15) Kurin-Csörgei, K.; Epstein, I. R.; Orbán, M. *J. Phys. Chem. A* **2006**, *110*, 7588–7592.
(16) Edblom, E. C.; Luo, Y.; Orbán, M.; Kustin, K.; Epstein, I. R. *J. Phys. Chem.* **1989**, *93*, 2722–2727.
(17) Packter, A.; Dhillon, H. S. *J. Chem. Soc. A* **1969**, 2588–2593.
(18) Dietzel, M.; Bohme, G. *Geochim. Cosmochim. Acta* **2005**, *69*, 1199–1211.
(19) Ermentrout, G. B. *XPPAUT*; Department of Mathematics, University of Pittsburgh: Pittsburgh, PA, 2008; see http://www.math.pitt.edu/~bard/xpp/xpp.html.
(20) Gayer, K. H.; Thompson, L. C.; Zajicek, O. T. *Can. J. Chem.* **1958**, *36*, 1268–1271.
(21) Bottero, J. Y.; Cases, J. M.; Fiessinger, F.; Poirier, J. E. *J. Phys. Chem.* **1980**, *84*, 2933–2939.
(22) Packter, A.; Chauhan, P.; Saunders, D. *Z. Phys. Chem.-Leipzig* **1969**, *242*, 289–601.
(23) Hanazaki, I.; Rábai, G. *J. Chem. Phys.* **1996**, *105*, 9912–9920.
(24) Rábai, G.; Kaminaga, A.; Hanazaki, I. *J. Phys. Chem.* **1996**, *100*, 16441–16442.
(25) Szanto, T. G.; Rábai, G. *J. Phys. Chem. A* **2005**, *109*, 5398–5402.
(26) Rábai, G.; Epstein, I. R. *Inorg. Chem.* **1989**, *28*, 732–736.
(27) Kaminaga, A.; Rábai, G.; Mori, Y.; Hanazaki, I. *J. Phys. Chem.* **1996**, *100*, 9389–9394.
(28) Antal, T.; Droz, M.; Magnin, J.; Racz, Z.; Zrinyi, M. *J. Chem. Phys.* **1998**, *109*, 9479–9486.
(29) Campbell, P. G. C.; Bisson, M.; Bougie, R.; Tessier, A.; Villeneuve, J. P. *Anal. Chem.* **1983**, *55*, 2246–2252.
(30) Doedel, E. *AUTO 07. Software for Continuation and Bifurcation Problems in Ordinary Differential Equations*; Computational Mathematics and Visualization Laboratory (CMVL), Department of Computer Science and Software Engineering, Concordia University: Montreal, Canada, 2008; see http://indy.cs.concordia.ca/auto. All computations were done with a tolerance of 10^{-4}.
(31) Jordan, J.; Ewing, G. J. *Inorg. Chem.* **1962**, *1*, 587–691.
(32) Baba, N.; Krischer, K. *Chaos* **2008**, *18*, 015103.
(33) Huh, D. S.; Choe, Y. M.; Park, D. Y.; Park, S. H.; Zhao, Y. S.; Kim, Y. J.; Yamaguchi, T. *Chem. Phys. Lett.* **2006**, *417*, 555–560.
(34) Kim, K. R.; Shin, K. J.; Lee, D. J. *J. Chem. Phys.* **2004**, *121*, 2664–2672.
(35) Sriram, K.; Gopinathan, M. S. *React. Kinet. Catal. Lett.* **2003**, *79*, 341–349.
(36) Strizhak, P. E.; Khavrus, V. O.; Bar-Eli, K. *J. Phys. Chem. A* **2002**, *106*, 2505–2511.
(37) Rachwalska, M.; Kawczynski, A. L. *J. Phys. Chem. A* **2001**, *105*, 7885–7888.
(38) Moller, A. C.; Lunding, A.; Olsen, L. F. *Phys. Chem. Chem. Phys.* **2000**, *2*, 3443–3446.
(39) Rachwalska, M.; Kawczynski, A. L. *J. Phys. Chem. A* **1999**, *103*, 3455–3457.
(40) Hauser, M. J. B.; Olsen, L. F. *J. Chem. Soc., Faraday Trans.* **1996**, *92*, 2857–2863.
(41) Neher, G.; Pohlmann, L.; Tributsch, H. *J. Phys. Chem.* **1995**, *99*, 17763–17771.
(42) Tracqui, P. *J. Nonlin. Sci.* **1994**, *4*, 69–103.
(43) Krischer, K.; Lubke, M.; Eiswirth, M.; Wolf, W.; Hudson, J. L.; Ertl, G. *Physica D* **1993**, *62*, 123–133.
(44) Koper, M. T. M.; Gaspard, P.; Sluyters, J. H. *J. Chem. Phys.* **1992**, *97*, 8250–8260.
(45) Koper, M. T. M.; Gaspard, P. *J. Chem. Phys.* **1992**, *96*, 7797–7813.
(46) Hudson, J. L.; Hart, M.; Marinko, D. *J. Chem. Phys.* **1979**, *71*, 1601–1606.
(47) Hauck, T.; Schneider, F. W. *J. Phys. Chem.* **1993**, *97*, 391–397.
(48) Dolnik, M.; Epstein, I. R. *J. Chem. Phys.* **1993**, *98*, 1149–1155.
(49) Rábai, G.; Hanazaki, I. *J. Phys. Chem.* **1996**, *100*, 15454–15459.
(50) Hauck, T.; Schneider, F. W. *J. Phys. Chem.* **1994**, *98*, 2072–2077.
(51) Tyson, J. J. *J. Chem. Phys.* **1975**, *62*, 1010–1015.
(52) Brons, M.; Bareli, K. *J. Phys. Chem.* **1991**, *95*, 8706–8713.
(53) Krupa, M.; Popovic, N.; Kopell, N. *SIAM J. Appl. Dynam. Syst.* **2008**, *7*, 361–420.
(54) Zagora, J.; Voslar, M.; Schreiberova, L.; Schreiber, I. *Phys. Chem. Chem. Phys.* **2002**, *4*, 1284–1291.

JP807840G